THE JOURNAL OF PHYSICAL CHEMISTRY C

Article

pubs.acs.org/JPCC

Optical Extinction Properties of Perforated Gold-Silica-Gold Multilayer Nanoshells

Jun Qian,[†] Wudeng Wang,[†] Yudong Li,[‡] Jingjun Xu,[‡] and Qian Sun[‡,*]

[†]School of Physics, Nankai University, Tianjin 300071, China

[‡]The Key Laboratory of Weak Light Nonlinear Photonics, Ministry of Education, Teda Applied Physics School, Nankai University, Tianjin 300457, China

Supporting Information

ABSTRACT: Symmetry breaking in gold nanoshell (or multilayer nanoshells) can supply many interesting optical properties, which has been studied in gold nanostrucutres such as nanocup, nanoegg, and core offset gold-silica-gold multilayer nanoshells. In this work, the optical extinction properties of the perforated gold-silica-gold multilayer nanoshells are studied by the discrete dipole approximation method simulations and plasmon hybridization theory. The extinction spectra of these particles are sensitive to the orientation of the particle with respect to polarization of the light due to the symmetry breaking. Because of the coupling of the plasmon resonance modes between the inner gold sphere and the outer nanocup structure, the perforated gold-silica-gold nanoshell provides the additional plasmon resonance peak and an even greater spectral tunability comparing with the nanocup of similar dimensions. By changing the geometry of the particles, the extinction peaks of the particles can be easily tuned into the near-infrared region, which is favorable for biological applications. The local refractive index sensitivity of the particles is also investigated, and the multiple extinction peaks simultaneous shift is found as surrounding medium is altered. The perforated gold-silica-gold multilayer nanoshells may provide various applications ranging from angularly selective filters to biological sensors.

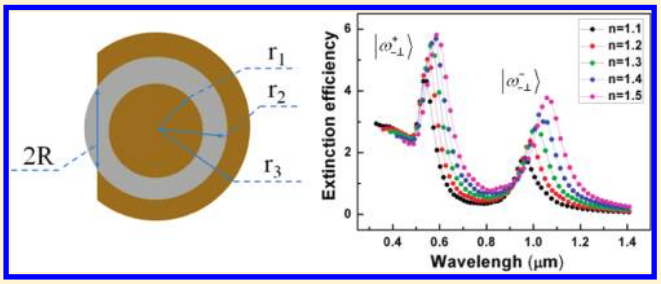

1. INTRODUCTION

Gold (Au) nanoshells consist of a dielectric core (typically silica) surrounded by an ultrathin Au shell and have generated great interest at present due to their highly tunable optical properties and plasmon resonances for a broad range of spectroscopic[1,2] and biomedical applications.[3−5] The plasmon resonances of Au nanoshells are greatly dependent on geometry and local dielectric environment. In Au nanoshells, the plasmon resonance can be tuned from visible to near-infrared region, which enables the various biomedical applications such as medical diagnostics[3,5] and biologic sensing,[6] by increasing the ratio of the core size to shell thickness.[7] To create a more abundant and tunable plasmon resonance band, an Au core has been inserted into the Au nanoshell to fabricate an Au-Silica-Au multilayer nanoshell.[8] In the Au-Silica-Au nanoshells, the interaction between the plasmon resonance mode of the inner Au sphere and the outer Au shell provides a high degree of plasmonic tunability, as explained by plasmon hybridization method.[9] The experimental synthesis[10] and theoretical investigations[11−13] of the multilayer Au-Silica-Au nanoshell have been reported in recent years.

Reducing the symmetry of Au nanoshells by excising a part of the nanoshell generates a series of semishells such as "nanocaps", "half-shells", and "nanocups".[14] Many of the interesting optical properties and applications originate with these reduced symmetries. The nanocups (or nanocaps) present the sensitive dependence of optical properties on the angle and polarization of the incident light.[14−17] As a result, arrays of these particles can serve as angularly and spectrally selective filters.[18] They also have a large field enhancement at the edge of the rim, which is useful in surface-enhance Raman spectroscopy (SERS) applications.[19−21] Furthermore, the nanocups have the unique ability to redirect scattered light at its resonant wavelength along its axis of symmetry.[22] Very recently, the nanocups have been demonstrated as highly efficient generators of second harmonic light.[23] The nanocup particles are usually prepared by two approaches:[24] the anisotropic etching of chemically synthesized nanoshells[15,16,19] and template deposition.[25−27] The anisotropic etching of Au nanoshell is like a perforation on the Au shell. The size and position of the hole on the shell can be well-controlled by the etching process.

Because the optical properties of nanocup are dependent on the angle and polarization of the incident light, there are two distinct bonding dipole resonances induced by different polarization of the incident light relative to the orientation of the particle.[16] One of them is usually called the axial mode (the polarization of the incident light is parallel to the axis of

Received: January 10, 2012
Revised: April 6, 2012
Published: April 17, 2012

symmetry), and the other is usually called the transverse mode (the polarization of the incident light is perpendicular to the axis of symmetry). The transverse mode plasmon resonance is always in larger wavelength region with respect to the axial mode plasmon resonance. It is found that the Au nanocup presents a more pronounced red shift of plasmon resonance (in transverse mode) and an enhanced local electromagnetic field compared with the Au nanoshell, which has great potential to surface-enhanced Raman spectroscopy (SERS)-based biomolecule detection and biosensing.[19] To obtain the plasmon resonance in the near-infrared (700−1300 nm) "Biological Window",[28] the size of the nanocup should be larger than 250 nm with the aspect ratio $R/(R - r) = 8.7$ and the fractional height $H/2R = 0.75$, where r is inner radius, R is outer radius, and H is cutoff height.[15] However, for some biomedical applications such as using nanoparticles as contrast agents, it is necessary to reduce the nanoshell's overall diameter to sub-100 nm region for facilitating their penetration into the biological tissues. In our opinion, an even better alternative is inserting an Au core into the Au nanocup. With an accessional Au core, the nanocups provide additional red shifts through plasmon hybridization while maintaining the small size and strong surface plasmon resonance (SPR). Such structures can be easily fabricated by the anisotropic etching method on the Au-silica-Au multilayer nanoshells. To our knowledge, there is no previous study on the influence of the geometry and local dielectric environment over the optical response of these perforated Au-silica-Au multilayer nanoshells.

In this Article, we study the influence of the inner core radius and outer nanoshell radius and the hole size on the optical properties of perforated Au-silica-Au multilayer nanoshells by using discrete dipole approximation (DDA) method. It is found that the optical properties of these structures are sensitive to the orientation of the particle with respect to polarization of the light, which is similar to the nanocups. However, the additional plasmon resonance peak and a greater spectral tunability are provided through plasmon hybridization compared with the nanocups. The local refractive index sensitivity of the particles is also investigated, and the multiple extinction peaks simultaneous shift is found as the surrounding medium changed. The structures we propose could provide an excellent substitute of nanocups for applications like biosensing and angularly selective filters. Furthermore, in the previous study, the plasmon hybridization theory is often used to describe the coupling of the plasmon resonance modes of symmetric nanostructures. In our work, the interaction of the plasmon resonance modes between the symmetric nanostructure (Au sphere) and the symmetry-breaking nanostructure (Au nanocup) is pictured by the plasmon hybridization theory, which might give new insight into the plasmon modes interaction of metal nanostructures.

2. THEORETICAL METHODS

Many theoretical approaches such as Mie theory,[29] finite-element method,[30] quasi-static theory,[31] and DDA method[32] have been developed to explain the SPR behavior of multishell metal-dielectric nanostructure. DDA method is a highly efficient and flexible technique to study the scattering and absorption of electromagnetic waves by targets with arbitrary geometries and complex refractive index. We have simulated the optical properties of the proposed perforated Au-silica-Au multilayer nanoshells using DDSCAT 7.1, the code of Draine and Flatau[33,34] that exploits the DDA method. In this scheme, the nanoparticle is represented by a 3-D array of dipoles, along with a radiative reaction correction. As a result, finite-size effects including electromagnetic retardation are taken into account, unlike in a purely dipolar model, where each particle is represented by a single dipole.[35] The applicability and accuracy of this code has been previously verified by various investigators.[36−38] The structure we propose is shown in Figure 1. The radii of the core, middle silica layer, and outer

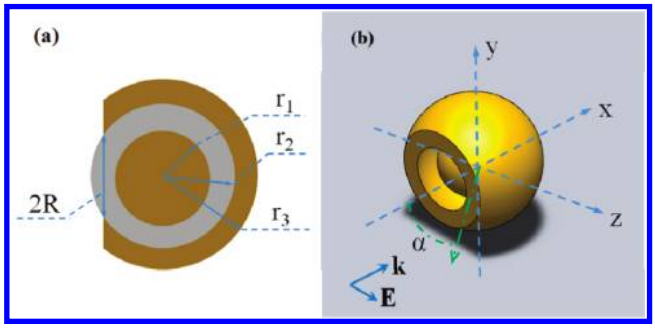

Figure 1. (a) Midsectional view of a perforated Au-silica-Au multilayer nanoshell. (b) Schematic of the perforated Au-silica-Au multilayer nanoshell in the rectangular coordinate system.

shell are r_1, r_2, and r_3. The radius of the hole is R. To investigate the angle and polarization dependence of incident light, we study the spectral properties of nanoshell in the rectangular coordinate system defined as a "Lab Frame" in the DDSCAT.[34] The incident radiation propagates in the $+x$ direction, and the polarization vector of incident light is along the z axis. The target nanoshell can easily be adjusted to arbitrary orientation relative to the incident light in the DDSCAT. The multilayer nanoshell structures with hole we studied are in the size region (diameter ∼100 nm), where successful particle fabrications have been reported.[10,16] In the calculations, the interdipole distance is taken equal to 2 nm, and dipole numbers between 50 000 and 134 000 are set for various nanoparticles. The surrounding medium is water. The dielectric properties for gold are taken from ref 39. The dielectric constant for silica is set to 2.04 and for water is 1.33.

The theory of plasmon hybridization theory[9] has been developed to understand the plasmon response of metallic nanoparticles. In this theory, the plasmon response of metal-based nanostructures can be explained in terms of the interaction of between the plasmons of metallic nanostructures in simpler forms. For example, the plasmon resonance of the metal nanoshell can be considered as the interaction between plasmons of a sphere $|\omega_S\rangle$ and a cavity $|\omega_C\rangle$. The hybridization of the sphere and cavity plasmons created two new plasmon oscillation modes, that is, the higher energy antibonding mode $|\omega_+\rangle$ and the lower energy bonding mode $|\omega_-\rangle$, corresponding to the antisymmetric and symmetric interactions between the $|\omega_S\rangle$ and $|\omega_C\rangle$ modes, respectively. Because of the hybridization between the additional Au core and the outer nanoshell plasmons, the tunability of plasmon resonances of Au-silica-Au multilayer nanoshell is much better than that of the Au nanoshell. The plasmon resonance in an Au-silica-Au multilayer nanoshell[11,13] can be viewed as the interaction between the plasmon modes of the inner core sphere ($|\omega_i\rangle$) and the outer nanoshell bonding ($|\omega_-^o\rangle$) and antibonding ($|\omega_+^o\rangle$) modes. The interaction of the nanoshell higher-energy antibonding modes $|\omega_+^o\rangle$ and the sphere mode $|\omega_i\rangle$ is weak and often unvisualized in spectrum.[8] Therefore, most of the previous studies are focused

dx.doi.org/10.1021/jp3003189 | J. Phys. Chem. C 2012, 116, 10349−10355

on the interaction between the lower energy bonding mode $|\omega_+^o\rangle$ and the sphere mode $|\omega_i\rangle$, which results in two hybridized plasmon modes. The lower energy mode $|\omega_-^-\rangle$ corresponded to an antisymmetric coupling, whereas the higher energy mode $|\omega_-^+\rangle$ corresponded to an symmetric coupling between the inner sphere mode $|\omega_i\rangle$ and the outer nanoshell mode $|\omega_-^o\rangle$.

Similar to the Au-silica-Au multilayer nanostructures, the plasmon resonance in the perforated Au-silica-Au multilayer nanoshells can be viewed as the interaction between plasmons supported by the inner Au sphere and the outer nanocup. As shown in Figure 2, we consider the interaction between the

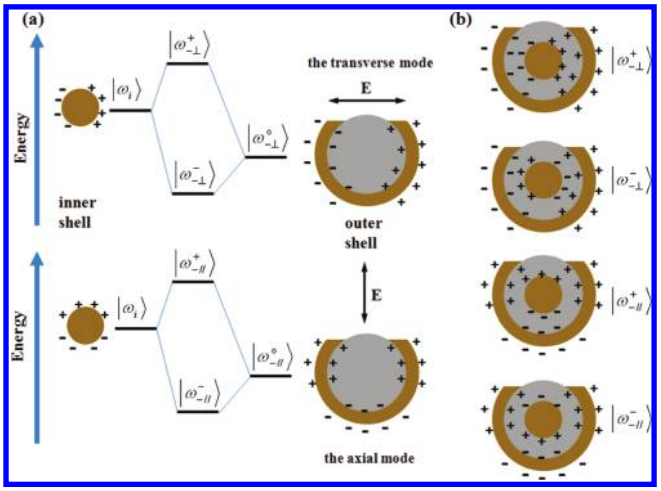

Figure 2. (a) Schematic of energy diagram of the inner Au core and outer nanocup, representing plasmon hybridization. (b) Schematic of the induced polarizations of the coupling modes of a perforated Au-silica-Au multilayer nanoshell.

sphere mode $|\omega_i\rangle$ and the transverse bonding mode $|\omega_{-\perp}^o\rangle$ of the nanocup and the sphere mode $|\omega_i\rangle$ and the axial bonding mode $|\omega_{-\parallel}^o\rangle$ of the nanocup, respectively. The energy mode $|\omega_{-\perp}^-\rangle$ ($|\omega_{-\perp}^+\rangle$) corresponds to the antisymmetric (symmetric) coupling between the sphere mode $|\omega_i\rangle$ and the transverse bonding mode $|\omega_{-\perp}^o\rangle$. The energy mode $|\omega_{-\parallel}^-\rangle$ ($|\omega_{-\parallel}^+\rangle$) corresponds to the antisymmetric (symmetric) coupling between the sphere mode $|\omega_i\rangle$ and the axial bonding mode $|\omega_{-\parallel}^o\rangle$. The symmetric coupling modes $|\omega_{-\perp}^+\rangle$ ($|\omega_{-\parallel}^+\rangle$) have a higher energy than the corresponding antisymmetric coupling modes $|\omega_{-\perp}^-\rangle$ ($|\omega_{-\parallel}^-\rangle$) due to the increased electrostatic repulsion at the internal adjacent interfaces occurring for those plasmon excitations.[40] The relative energies of the hybrid modes can be tuned by the controlling the strength of the interaction between the core and the nanocup plasmons, which is often achieved by controlling the thickness of the dielectric layer between the Au core and Au nanocup.

3. RESULTS AND DISCUSSION

We first consider the Au nanocup with $r_1/r_2/r_3$ = 0, 38, 50 nm and R = 16 nm, as shown in Figure 1. It is seen that the axis of the symmetry of the nanocup is the x axis. When we rotate the nanoshell along the y axis, the angle between the E field and symmetry axis of the particle is also changed, which influences the extinction spectrum of the particle, as shown in Figure 3a. Because the optical extinction spectrum of the Au semishells is mainly determined by the direction of the polarization vector and is almost independent of the direction of the k vector of the incident light,[14,16] we considered only the acute angle α, as

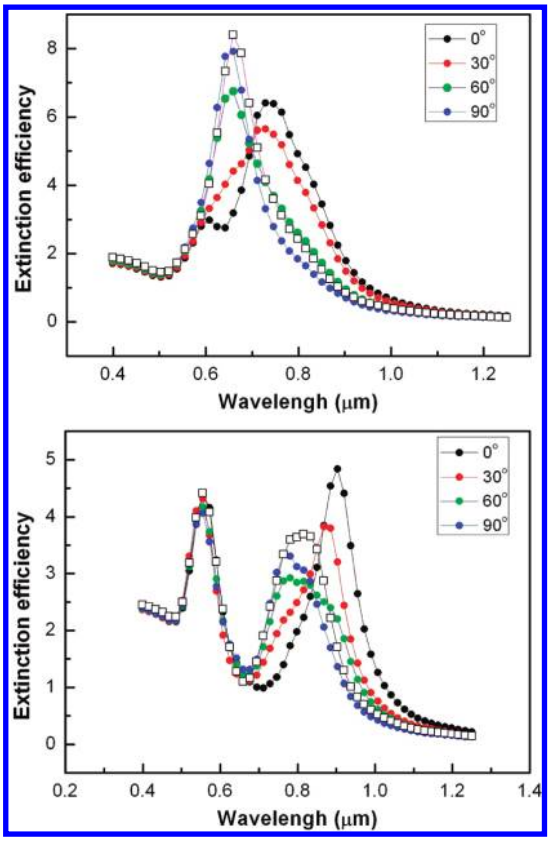

Figure 3. (a) Extinction efficiency of the nanocup ($r_1/r_2/r_3$ = 0, 38, 50 nm; R = 16 nm) at the rotational angle α = 0, 30, 60, 90° along y axis (filled circles) and extinction efficiency of the nanoshell without hole ($r_1/r_2/r_3$ = 0, 38, 50 nm, open squares). (b) Extinction efficiency of the perforated Au-silica-Au multilayer nanoshell ($r_1/r_2/r_3$ = 26, 38, 50 nm; R = 16 nm) at the rotational angle α = 0, 30, 60, 90° along y axis (filled circles) and extinction efficiency of the Au-silica-Au multilayer nanoshell without hole ($r_1/r_2/r_3$ = 26, 38, 50 nm, open squares).

shown in Figure 1b. In Figure 3a, we show the extinction spectrum of the nanoshell when the particle rotates along y axis at α = 0, 30, 60, 90°. It is seen that the extinction peak at 764 nm weakens and disappears and the extinction peak at 642 nm emerges as the particle rotates from 0 to 90°. The resonance at 642 nm (α = 90°) is the axial mode ($|\omega_{-\parallel}^o\rangle$), where the E field is parallel to the axis of symmetry, and the resonance at 764 nm (α = 0°) is the transverse mode ($|\omega_{-\perp}^o\rangle$), where the E field is perpendicular to the axis of rotational symmetry. Next, by inserting an Au sphere into the nanocup, we consider the perforated Au-silica-Au multiplayer nanoshells with $r_1/r_2/r_3$ = 26, 38, 50 nm and R = 16 nm. Figure 3b shows the extinction spectrum of this nanoshell when the particle rotates along the y axis at α = 0, 30, 60, 90°. We find that, similar to nanocups, the extinction spectrum of perforated Au-silica-Au multiplayer nanoshells is also sensitive to the orientation of the particle with respect to polarization of the light. It is seen that both the transverse mode ($|\omega_{-\perp}^o\rangle$) and the axial mode ($|\omega_{-\parallel}^o\rangle$) of the nanocup shown in Figure 3a split by interaction with the inner sphere mode $|\omega_i\rangle$, as shown in Figure 3b. The corresponding new antisymmetric (symmetric) coupling modes $|\omega_{-\perp}^-\rangle$ ($|\omega_{-\perp}^+\rangle$) ($\alpha$ = 0° in Figure 3b) and $|\omega_{-\parallel}^-\rangle$ ($|\omega_{-\parallel}^+\rangle$) ($\alpha$ = 90° in Figure 3b) are created. The antisymmetric coupling mode $\omega_{-\perp}^-$ between the transverse mode $|\omega_{-\perp}^o\rangle$ and the sphere mode $|\omega_i\rangle$ is moved in the near-infrared region. As the particle rotates along y axis at α = 0, 30, 60, 90°, the angle between the E field and symmetry

dx.doi.org/10.1021/jp3003189 | J. Phys. Chem. C 2012, 116, 10349−10355

axis of the outer nanocup is changed, which results in the blue shift of the lower energy antisymmetric coupling modes like the changing of the bonding mode of the nanocup in Figure 3a, but the higher energy symmetric coupling modes are almost unchanged. It is similar to the plasmon hybridization in Au-silica-Au nanoshell[11] that the $|\omega^-_-\rangle$ mode is more sensitive to the bonding mode $|\omega^o_-\rangle$ of outer nanoshell, whereas the $|\omega^+_-\rangle$ mode is more dependent on the mode $|\omega_i\rangle$ of inner core. The extinction spectra of the nanoshell ($r_1/r_2/r_3$ = 0, 38, 50 nm) and multiplayer nanoshells ($r_1/r_2/r_3$ = 26, 38, 50 nm) without symmetry breaking are also shown in Figure 3a,b (open squares in Figure 3). Comparing with the corresponding structures with symmetry breaking, they do not have the polarization sensitivity of the incident light.

In the following, we investigated the geometrical tunability of the optical properties of perforated Au-silica-Au multilayer nanoshells. For simplicity, we only consider the coupling modes between the transverse (axial) mode $|\omega^o_{-\perp}\rangle$ ($|\omega^o_{-\parallel}\rangle$) and the sphere mode $|\omega_i\rangle$, that is, when the particle rotates along y axis at α = 0 and 90°. We briefly name them as transverse mode coupling (α = 0°) and axial mode coupling (α = 90°) in the following. We first consider the dependence of the core radius r_1 and shell radius r_3 on the optical properties of particles when the radius of hole R is fixed. Figure 4 shows the extinction spectrum of perforated Au-silica-Au multilayer nanoshells with r_1 = 18, 22, 26, 30 nm at r_2 = 38 nm, r_3 = 50 nm, and R = 16 nm. The transverse coupling modes of $|\omega^-_{-\perp}\rangle$ ($|\omega^+_{-\perp}\rangle$) are shown in Figure 4a, and the axial coupling modes of $|\omega^-_{-\parallel}\rangle$ ($|\omega^+_{-\parallel}\rangle$) are shown in Figure 4b. An increase in the inner Au core radius will decrease the intermediate silica layer thickness and increase the plasmon interaction between the Au core and the outer nanocup. This is accompanied by a red shift of both the antisymmetric and symmetric coupling modes, as shown in Figure 4a,b. Our results agree with the report of Hu et al.[12] on the Au-silica-Au multiplayer shell. However, Wu et al.[11] found that increasing of the core radius leads to the $|\omega^-_-\rangle$ mode red shift but the $|\omega^+_-\rangle$ mode blue shift in the Au-silica-Au multiplayer shell. In a very recent report, Zhu et al.[13] demonstrated that with the increase in core radius the $|\omega^-_-\rangle$ mode always red shifts but the change of the $|\omega^+_-\rangle$ mode depends on the dielectric constant of the middle dielectric layer and the local environment. It is also seen that the extinction peaks of the $|\omega^-_-\rangle$ mode can be easily tuned in the near-infrared region by changing the radius of Au core.

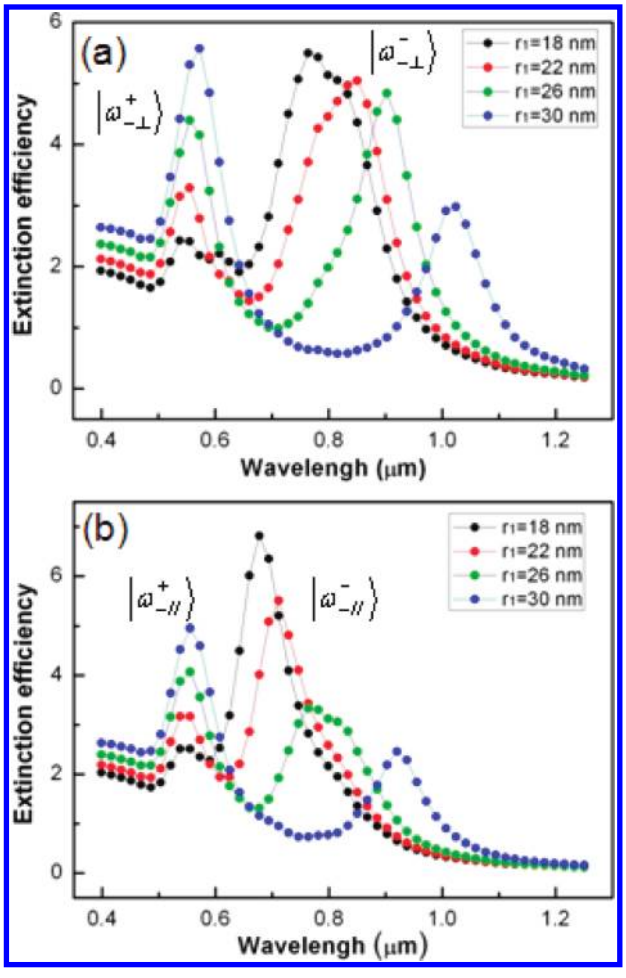

Figure 4. Extinction efficiency of the perforated Au-silica-Au multilayer nanoshell with different r_1 (r_1 = 18, 22, 26, 30 nm; r_2/r_3 = 38, 50 nm; R = 16 nm) at the rotational angle α = 0° (a) and α = 90° (b) along y axis.

The electromagnetic retardation effects could manifest and result in direct excitation of higher-order modes when particle size is comparable to the wavelength of incident light. It was found that with the symmetry breaking some higher-order modes appear in the spectrum in the nanocup because of the retardation effects.[16] In simulations, we also find that the modes due to the retardation effects can appear and result in the broad resonant peaks by superposition of dipolar modes (in the Supporting Information).

In Figure 5, we show the extinction spectrum of perforated Au-silica-Au multilayer nanoshells with r_3 = 50, 56, 62, 68 nm at r_1 = 26 nm, r_2 = 38 nm, and R = 16 nm. It is seen that the antisymmetric coupling modes $|\omega^-_{-\perp}\rangle$ ($|\omega^-_{-\parallel}\rangle$) blue shift and the symmetric coupling modes $|\omega^+_{-\perp}\rangle$ ($|\omega^+_{-\parallel}\rangle$) red shift with increase in shell thickness. The increase in shell thickness should decrease the ratio of the inner and outer radii of the nanocup shell and hence increase the resonance energy for the $|\omega^o_-\rangle$ mode of nanocup shell.[38] In this case, the resonance energy of the coupled $|\omega^-_-\rangle$ and $|\omega^+_-\rangle$ modes should be increased. The increase in shell thickness equivalently increases the interval between the Au core and Au nanoshell and thus reduces the coupling strength between the core and the outer shell. Therefore, the energy separation between the $|\omega^-_-\rangle$ mode and $|\omega^+_-\rangle$ mode is decreased, which results in the increase in the energy of $|\omega^-_-\rangle$ mode and the decrease in the energy of $|\omega^+_-\rangle$ mode. In both cases, the energy of $|\omega^-_-\rangle$ mode is increased. However, for the coupled $|\omega^+_-\rangle$ mode, when the interval between the Au core and Au nanoshell is not very large, the influence of the variation of coupling strength is stronger than that due to the variation of the $|\omega^o_-\rangle$ mode.[11] Therefore, the decreased resonance energy for $|\omega^+_-\rangle$ mode happens.

Second, we study the influence of the radius of hole R (R = 16, 26, 32, 36 nm) on the optical properties of particles when the radii of core r_1, middle silica layer r_2, and outer shell r_3 are fixed ($r_1/r_2/r_3$ = 26, 38, 50 nm). Figure 6a,b shows transverse mode coupling $|\omega^-_{-\perp}\rangle$ ($|\omega^+_{-\perp}\rangle$) and axial mode coupling $|\omega^-_{-\parallel}\rangle$ ($|\omega^+_{-\parallel}\rangle$), respectively. As the previous paper shows,[14,15] with the increase in hole size, the energy of the transverse modes $|\omega^o_{-\perp}\rangle$ of nanocup reduces and the mode $|\omega^o_{-\perp}\rangle$ red shifts, whereas the energy of the axial modes $|\omega^o_{-\parallel}\rangle$ of nanocup increases and the mode $|\omega^o_{-\parallel}\rangle$ blue shifts. In addition, the antisymmetric coupling modes $|\omega^-_{-\perp}\rangle$ and $|\omega^-_{-\parallel}\rangle$ are more sensitive to the outer nanoshell, whereas the symmetric coupling modes $|\omega^+_{-\perp}\rangle$ and

dx.doi.org/10.1021/jp3003189 | J. Phys. Chem. C 2012, 116, 10349−10355

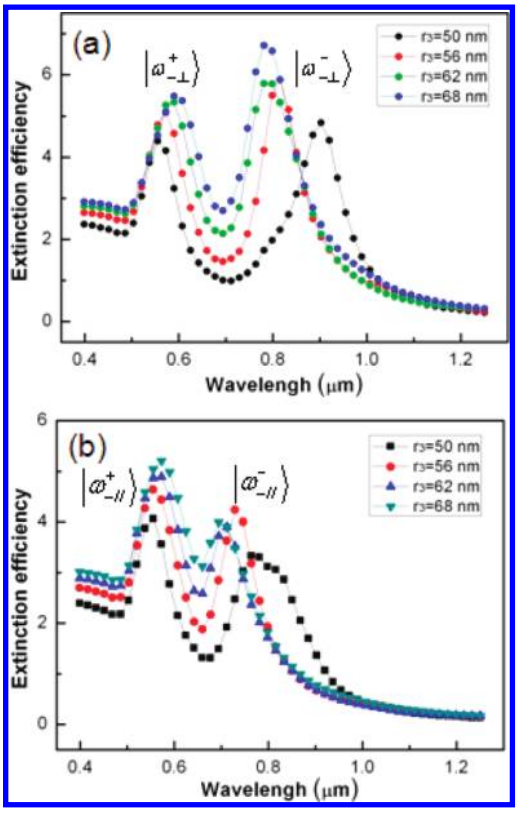

Figure 5. Extinction efficiency of the perforated Au-silica-Au multilayer nanoshell with different r_3 (r_3 = 50, 56, 62, 68 nm; r_1/r_2 = 26, 38 nm; R = 16 nm) at the rotational angle α = 0° (a) and α = 90° (b) along y axis.

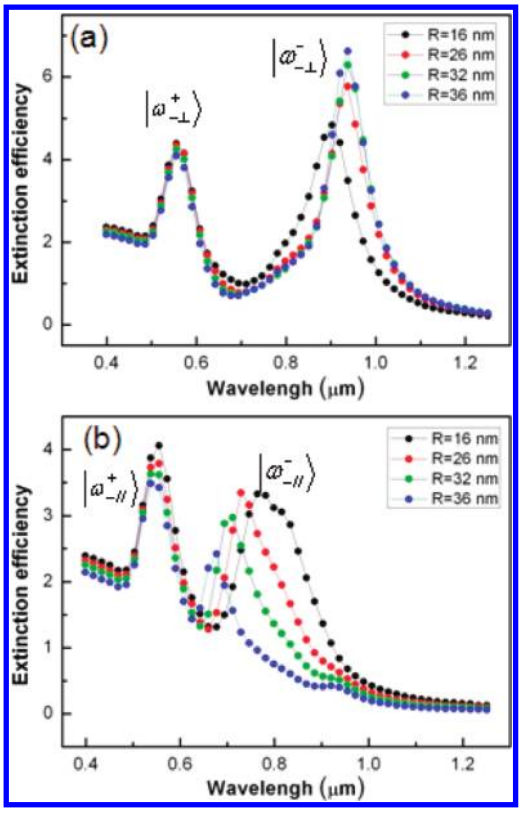

Figure 6. Extinction efficiency of the perforated Au-silica-Au multilayer nanoshell with different R (R = 16, 26, 32, 36 nm; $r_1/r_2/r_3$ = 26, 38, 50 nm) at the rotational angle α = 0° (a) and α = 90° (b) along y axis.

$|\omega^+_{-\parallel}\rangle$ are more dependent on the inner core.[11] Therefore, the antisymmetric coupling mode $|\omega^-_{-\perp}\rangle$ red shifts and $|\omega^-_{-\parallel}\rangle$ blue shifts, but the symmetric coupling modes $|\omega^+_{-\perp}\rangle$ and $|\omega^+_{-\parallel}\rangle$ are almost unchanged with the increase in hole size, as shown in Figure 6. Note that for the transverse mode of the nanocup the opposite charges accumulate on opposing edges of the cup opening.[16] Increasing the size of the cup opening leads to the enhancement of dipole moment of the transverse mode and hence increases the extinction peak value of the transverse mode, as shown in ref 14. Similar to the nanoshell,[41,42] the lower energy mode $|\omega^-_{-\perp}\rangle$ has a stronger admixture of $|\omega^o_{-\perp}\rangle$ mode, and the higher energy mode $|\omega^+_{-\perp}\rangle$ has a stronger admixture of the mode $|\omega_i\rangle$. Therefore, it could be seen that the amplitude of the antisymmetric coupling modes $|\omega^-_{-\perp}\rangle$ increases even larger than the symmetric coupling modes $|\omega^+_{-\perp}\rangle$ with the increase in hole radius R, as shown in Figure 6a. The electric field profiles of nanoparticles with different geometries are also calculated (in the Supporting Information); it is seen that in the $|\omega^-_{-\perp}\rangle$ modes the distribution of hotspots is usually in the outer shell, which is more potential for the applications such as SERS and localized SPR biosensor.

Furthermore, we investigate the spectral sensitivity of perforated Au-silica-Au multilayer nanoshells ($r_1/r_2/r_3$ = 30, 38, 50 nm; R = 16 nm) to the surrounding medium. Figure 7a,b shows transverse mode coupling $|\omega^-_{-\perp}\rangle$ ($|\omega^+_{-\perp}\rangle$) and axial mode coupling $|\omega^-_{-\parallel}\rangle$ ($|\omega^+_{-\parallel}\rangle$), respectively. We found that an increase in the refractive index of the medium results in an overall red shift of spectrum, as demonstrated in Figure 7. Multiple extinction peaks are shifted synchronously when the surrounding medium is perturbed. The antisymmetric coupling modes of $|\omega^-_{-\perp}\rangle$ and $|\omega^-_{-\parallel}\rangle$ in Figure 7a,b are properly located in the near-infrared region, which suggests the potential bioapplications.

4. CONCLUSIONS

In this Article, we study the optical extinction properties of the perforated Au-silica-Au multilayer nanoshells in both transverse mode and axial mode coupling by DDA simulations. We show that the extinction peaks of the particles can be easily tuned into the near-infrared region by change the geometry of the particles. The coupling of the plasmon resonance modes between the symmetric Au sphere and the symmetry-breaking nanocup structure is explained through the plasmon hybridization pictures. With an increase in inner core radius, the antisymmetric coupling modes $|\omega^-\rangle$ and the symmetric coupling modes $|\omega^+\rangle$ red shift in transverse mode and axial mode couplings due to the increase in the coupling strength between plasmon modes of the Au core and the outer nanocup. Because of the reduction of the interaction between the Au core and the outer nanocup and the decrease in the ratio of the inner and outer radii of the nanocup as the thickness of the outer shell is increased, the antisymmetric coupling modes $|\omega^-\rangle$ blue shift and the symmetric coupling modes $|\omega^+\rangle$ red shift in the extinction spectrum. Moreover, with an increase in hole size, the antisymmetric coupling modes $|\omega^-\rangle$ show a red shift (blueshift) in transverse (axial) mode coupling, which is similar to the plasmon response of nanocup. We also investigate local refractive index sensitivity of the particles and find the multiple extinction peaks simultaneous shift as the surrounding medium altered. The perforated Au-silica-Au multilayer nanoshells that

dx.doi.org/10.1021/jp3003189 | J. Phys. Chem. C 2012, 116, 10349−10355

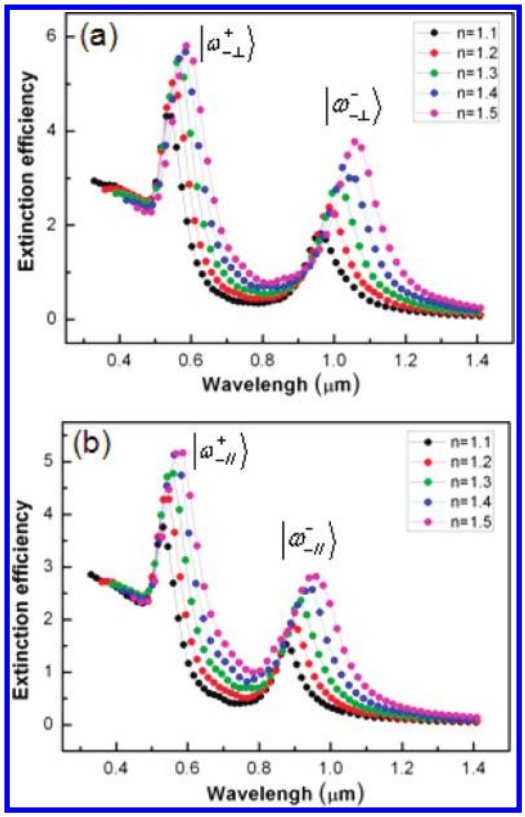

Figure 7. Local refractive index sensitivity of the perforated Au-silica-Au multilayer nanoshell ($r_1/r_2/r_3$ = 30, 38, 50 nm; R = 16 nm) at the rotational angle α = 0° (a) and α = 90° (b) along y axis.

show better tunability of plasmon resonance over the nanocup may provide the various applications ranging from novel optical devices to biological sensors.

■ ASSOCIATED CONTENT

Supporting Information

Electric field profiles of nanoparticles with different geometries and quasistatic simulations of several structures. This material is available free of charge via the Internet at http://pubs.acs.org.

■ AUTHOR INFORMATION

Corresponding Author

*E-mail: qiansun@nankai.edu.cn. Tel: 86-022-23506238. Fax: 86-022-23506238.

Notes

The authors declare no competing financial interest.

■ ACKNOWLEDGMENTS

This work is supported by National Natural Science Foundation of China (60978020, 61178004), Natural Science Foundation of Tianjin (06TXTJJC13500), Program for Changjiang Scholars and Innovative Research Team in Nankai University, and the Fundamental Research Funds for the Central Universities.

■ REFERENCES

(1) Levin, C. S.; Kundu, J.; Barhoumi, A.; Halas, N. J. *Analyst* **2002**, *134*, 17451750.
(2) Mayer, K. M.; Hafner, J. H. *Chem. Rev.* **2010**, *111*, 3828−3857.
(3) Bikram, M.; Gobin, A. M.; Whitmire, R. E.; West, J. L. *J. Controlled Release* **2007**, *123*, 219−227.
(4) Park, J.; Estrada, A.; Sharp, K.; Sang, K.; Schwatz, J. A.; Smith, D. K.; Coleman, C.; Payne, J. D.; Korgel, B. A.; Dunn, A. K.; Tunnell, J. W. *Opt. Express* **2008**, *16*, 1590−1599.
(5) Lowery, A. R.; Gobin, A. M.; Day, E. S.; Halas, N. J.; West, J. L. *Int. J. Nanomed.* **2006**, *1*, 149−154.
(6) Raschke, G.; Brogl, S.; Susha, A. S.; Rogach, A. L.; Klar, T. A.; Feldmann., J. *Nano Lett.* **2004**, *4*, 1853−1857.
(7) Westcott, S. L.; Jackson, J. B.; Radloff, C.; Halas, N. J. *Phys. Rev. B* **2002**, *66*, 155431.
(8) Bardhan, R.; Mukherjee, S.; Mirin, N. A.; Levit, S. D.; Nordlander, P.; Halas, N. J. *J. Phys. Chem. C* **2010**, *114*, 7378−7383.
(9) Prodan, E.; Radloff, C.; Halas, N. J.; Nordlander, P. *Science* **2003**, *302*, 419−422.
(10) Xia, X. H.; Liu, Y.; Backman, V.; Ameer, G. A. *Nanotechnology* **2006**, *17*, 5435−5440.
(11) Wu, D. J.; Liu, X. J. *Appl. Phys. B: Laser Opt.* **2009**, *97*, 193−197.
(12) Hu, Y.; Fleming, R. C.; Drezek, R. A. *Opt. Express* **2008**, *16*, 19579−19591.
(13) Zhu, J.; Li, J. J.; Zhao, J. W. *Plasmonics* **2011**, *6*, 527−534.
(14) Cortie, M.; Ford, M. *Nanotechnology* **2007**, *18*, 235704.
(15) Ye, J.; Dorpe, P. V.; Roy, W. V.; Lodewijks, K.; Vlaminck, I. D.; Maes, G.; Borghs, G. *J. Phys. Chem. C* **2009**, *113*, 3110−3115.
(16) Lassiter, J. B.; Knight, M. W.; Mirin, N. A.; Halas, N. J. *Nano Lett.* **2009**, *9*, 4326−4332.
(17) Ye, J.; Lagae, L.; Maes, G.; Borghs, G.; Dorpe, P. V. *Optics Express* **2009**, *17*, 23765−23771.
(18) Liu, J.; Cankurtaran, B.; Wieczorek, L.; Ford, M. J.; Cortie, M. *Adv. Funct. Mater.* **2006**, *16*, 1457−1461.
(19) Ye, J.; Dorpe, P. V.; Roy, W.;V.; Borghs, G.; Maes, G. *Langmuir* **2009**, *25*, 1822−1827.
(20) Lu, Y.; Liu, G. L.; Kim, J.; Mejia, Y. X.; Lee, L. P. *Nano Lett.* **2005**, *5*, 119−124.
(21) Ye, J.; Chen, C.; Lagae, L.; Maes, G.; Borghs, G.; Van Dorpe, P. *Phys. Chem. Chem. Phys.* **2010**, *12*, 11222−11224.
(22) Zhang, Y.; Barhoumi, A.; Lassiter, J. B.; Halas, N. J. *Nano Lett.* **2011**, *11*, 1838−1844.
(23) Zhang, Y.; Grady, N. K.; Orozco, C. A.; Halas, N. J. *Nano Lett.* **2011**, *11*, 5519−5523.
(24) Van Dorpe, P.; Ye, J. *ACS Nano* **2011**, *5*, 6774−6778.
(25) Charnay, C.; Lee, A.; Man, S.; Moran, C. E.; Radloff, C.; Bradley, R. K.; Halas, N. J. *J. Phys. Chem. B* **2003**, *107*, 7327−7333.
(26) Love, J. C.; Gates, B. D.; Wolfe, D. B.; Paul, K. E.; Whitesides, G. M. *Nano Lett.* **2002**, *2*, 891−894.
(27) Ye, J.; Verellen, N.; Van Roy, W.; Lagae, L.; Maes, G.; Borghs, G.; Van Dorpe, P. *ACS Nano* **2010**, *4*, 1457−1464.
(28) Smith, A. M.; Mancini, M. C.; Nie, S. *Nat. Nanotechnol.* **2009**, *4*, 710−711.
(29) Peña-Rodríguez, O.; Pal, U. *J. Phys. Chem. C* **2010**, *114*, 4414−4417.
(30) Hu, Y.; Noelck, S. J.; Drezek, R. A. *ACS Nano* **2010**, *4*, 1521−1528.
(31) Haus, J. W.; Zhou, H. S.; Takami, S.; Hirasawa, M.; Honma, I.; Komiyama, H. *J. Appl. Phys.* **1993**, *73*, 1043−1048.
(32) Kelly, K. L.; Coronado, E.; Zhao, L. L.; Schatz, G. C. *J. Phys. Chem. B* **2003**, *107*, 668−677.
(33) Draine, B. T.; Flatau, P. J. *J. Opt. Soc. Am. A* **1994**, *11*, 1491−1499.
(34) Draine, B. T.; Flatau, P. J. User guide to the Discrete Dipole Approximation Code DDSCAT 7.1, 2010
(35) Gunnarsson, L.; Rindzevicius, T.; Prikulis, J.; Kasemo, B.; Kall, M.; Zou, S.; Schatz, G. C. *J. Phys. Chem. B* **2005**, *109*, 1079−1087.
(36) Yang, W. H.; Schatz, G. C.; Van Duyne, R. P. *J. Chem. Phys.* **1995**, *103*, 869−875.
(37) Yang, P.; Portales, H.; Pileni, M. P. *J. Phys. Chem. C* **2009**, *113*, 11597−11604.
(38) Hao, E.; Li, S.; Bailey, R. C.; Zou, S.; Schatz, G. C.; Hupp, J. T. *J. Phys. Chem. B* **2004**, *108*, 1224−1229.
(39) Johnson, P. B.; Christy, R. W. *Phys. Rev. B: Condens. Matter Mater. Phys.* **1972**, *6*, 4370−4379.

(40) Radloff, C.; Halas, N. J. *Nano Lett.* **2004**, *4*, 1323−1327.
(41) Prodan, E.; Lee, A.; Nordlander, P. *Chem. Phys. Lett.* **2002**, *360*, 325−332.
(42) Park, T. H.; Nordlander, P. *Chem. Phys. Lett.* **2009**, *472*, 228−231.